Coupled Quantum - Scattering Modeling of Thermoelectric Properties of Si/Ge/Si Quantum Well Superlattice

A. Bulusu
Graduate Research Assistant
Interdisciplinary Program in Material Science
Vanderbilt University
Nashville, TN 37235
anuradha.bulusu@vanderbilt.edu

D. G. Walker[1]
Assistant Professor
Department of Mechanical Engineering
Vanderbilt University
Nashville, TN 37235
greg.walker@vanderbilt.edu

Confined structures presumably offer enhanced performance of thermoelectric devices. 1) Interfaces and boundaries create scattering sites for phonons, which reduces the thermal conductivity. 2) Reduced dimensionality increases the local density of states near the Fermi level, which increases the Seebeck coefficient. From these two phenomena, the net effect should be an increase in ZT, the performance parameter used to evaluate different materials and structures. These effects have been measured and modeled, but none of the models attempts to quantify the electron-phonon coupled effects particularly in the regime where quantum and scattering influences are found. Using the non-equilibrium Green's function (NEGF) approach, quantum wells composed of Si and Ge are studied and the important physics isolated. Results show a competing effect between the decrease in the electrical conductivity due to scattering with the increase in electrical conductivity with doping, leading to 77% decrease in the value of the power factor for the case of electron-optical phonon scattering.

INTRODUCTION

The usefulness of thermoelectric materials is often characterized by the dimensionless thermoelectric figure of merit $ZT = S^2\sigma T/\kappa$ where S is the Seebeck coefficient, σ is the electrical conductivity and κ is the thermal conductivity. Research has been focused towards developing materials that have a high Seebeck coefficient as well as structures that will either have reduced thermal conductivity or enhanced electrical conductivity resulting in an increase in ZT [1]. In the past decade, the use of confined structures such as quantum well and quantum wire superlattices have gained attention as thermoelectric materials due to a number of advantages [2, 3, 4]. The reduced dimensionality of quantum well superlattices increases the local density of density of states per unit volume near the Fermi energy leading to an increase in the Seebeck coefficient [5]. The reduced dimensionality also causes phonon confinement leading to reduced thermal conductivity [6, 7]. In addition, the presence of material interfaces in the superlattice promotes phonon scattering, which theoretically reduces the effective thermal conductivity [2, 3, 4]. Phonon interference effects caused by phonon-interface scattering give rise to bandgaps at the interface of the thin films affecting phonon transport through these structures [8].

Chen [9, 10] studied phonon transport in Si/Ge superlattices using the BTE for phonons. Phonon interface scattering was included through a combination of diffuse and specular scattering. He found that the greatest temperature drop occurred at the interfaces rather than within the layers due to a combination of diffuse and inelastic scattering processes thus

developing the concept of phonon engineering to build structures having low thermal conductivity. However, experimental observations have not been able to achieve the presumed benefits of superlattice thermoelectric devices despite a theoretically predicted and experimentally observed reduction in the thermal conductivity of a superlattice compared to its bulk counterpart [5, 11]. While phonon confinement and scattering leads to reduced thermal conductivity, the electrical conductivity is assumed not to be significantly affected due to the large semiconductor bandgap and the disparity between the electron and phonon mean free paths [12]. However, this assumption does not take into consideration the effects of electron confinement as well as electron-phonon interaction due to phonon scattering processes. Hence there is a need to better understand the effect of the other significant factor contributing to the thermoelectric figure of merit of nanoscale devices namely the electrical conductivity σ.

The two fundamental aspects that differentiate nanoscale devices from bulk devices are scattering effects and quantum effects. Scattering in nanostructures can significantly affect carrier as well as thermal transport in devices [14]. Inelastic electron-phonon scattering causes electrons to lose or gain energy with the lattice while other scattering effects such as carrier-carrier, carrier-defect, and carrier-boundary scattering can lead to energy redistribution in devices where transport is near ballistic. Quantum effects manifest themselves in the form of electron tunneling as well as carrier confinement [14]. These effects usually dominate when the device length scales are of the order of the de Broglie wavelength associated with the device. Quantum confinement can lead to reduced density of

---

[1] Corresponding author

states available for the carrier while electron tunneling can have a detrimental impact in the form of leakage currents in very small sized transistors [15]. However, quantum effects can be leveraged as a high performance alternative to very-large-scale integration (VLSI) [16] in the form of resonant tunneling diodes. Shrinking device dimensions present an increasing need for a simple transport model that can effectively couple quantum with scattering effects. The need to incorporate scattering stems from the fact that while electron-phonon scattering usually helps restore thermodynamic equilibrium, shrinking device dimensions may not ensure enough scattering to restore equilibrium. The simultaneous consideration of scattering effects, which is usually described as particle behavior, and quantum effects, which are wave in nature, is extremely difficult and computationally intensive.

Classical transport models

In general carrier transport models can be classified into two types. The first type is the classical particle models that are based on finding the solution to the Boltzmann transport equation (BTE). The BTE based models allow for the inclusion of limited carrier scattering through a relaxation-time approximation treating the system to be only slightly perturbed from equilibrium. Numerical solutions to the BTE are possible using Monte Carlo techniques [17] in which particle distributions are solved using stochastic processes. Mazumder et al. [18] describes such an approach that includes phonon dispersion and various phonon modes independently. For coupled solutions, an electro-thermal model based on moments of the BTE for phonons and electrons was developed to simulate electron-phonon interactions [19]. This non-equilibrium approach has shown that the energy distributions for optical and acoustic phonons differ significantly suggesting that non-equilibrium behavior is very different from continuum behavior. Using a similar model, Raman [20] showed that non-equilibrium significantly affects the location and generation of the hot spot in microelectronic power devices. To remove the gray assumption in moment-based solutions, an unstructured finite-volume discrete ordinates scheme has been used by several groups to solve the BTE with spectral information [21]. Isotropic scattering in the form of impurity and Umklapp scattering was considered and a favorable match with exact solutions was found.

Quantum effects in the BTE based models are included by incorporating a quantum correction to the transport model. Common methods of incorporating quantum effects are the density gradient formalism and the effective potential method [22]. The density gradient formalism is derived from the equation of motion for the one particle Wigner function where quantum corrections are introduced by expressing the mean potential energy as a power series in h. The transport equation for the Wigner distribution function can now be written in the form of a modified Boltzmann Transport Equation. In the effective potential method a spatially-localized wave packet is used as a representation of the electron where the size of the wave packet is defined roughly by the thermal de Broglie wavelength. The non-local form of the charge distribution introduces an effective potential when the inhomogeneous potential is introduced in the Hamiltonian. The generation of the effective potential determines the onset of quantization in the system due to the non-local nature of the potential. The quantum correction methods have been found to give an excellent match with the Poisson-Schrodinger solver for the case of carrier confinement and tunneling. More recently, attempts have been made to combine quantum corrections with the Monte Carlo technique [23] which is a numerical solution to the BTE. The results have been found to match well with the Schrödinger solution in the case of carrier confinement while a reasonably close match was observed for the case of tunneling. However, extension of this model to 2 and 3 dimensions remains, computationally tedious and difficult.

Quantum transport models

The second approach to modeling carrier transport consists of quantum wave function models that involve the solution to the Schrödinger wave equation. These models can be used to study current flow over small scales where the transport can be either ballistic or can involve some type of scattering. The main models used to model ballistic transport are Quantum Transmitting Boundary Model (QTBM) [24] and the Quantum Device Analysis by Mode Evaluation (QDAME) [25]. QTBM involves formulating the boundary conditions for a given problem by calculating the transmission and reflection coefficients for a known boundary potential. These boundary conditions are then used in a discretized solution to obtain the wave function over the entire problem domain. While this method is suitable for solving the Schrödinger equation for various boundary potentials, inclusion of dissipation due to scattering becomes very difficult. QDAME involves discretely sampling a device's density of states using standing wave boundary conditions. The standing waves are decomposed into traveling waves and injected from the contacts from which their occupancies are assigned. All-in-all, in spite of all the progress made in small scale device modeling the fact remains that rigorous scattering cannot be fully included in most models and coupling scattering models to quantum models continues to remain extremely challenging.

The non-equilibrium Green's function formalism provides a framework for natural coupling of quantum and scattering effects. Open boundary conditions allow the source and drain contacts to be coupled to the device through simple self-energy terms that helps eliminate working with huge matrices that are of the size of the source and drain reservoir systems and instead work with matrices that are the size of the device Hamiltonian. In addition, the NEGF formalism allows for the rigorous incorporation of both elastic and inelastic scattering effects using the concept of Buttiker probes where scattering is treated as another contact, allowing it to be coupled to the device using self-energy terms. We present a brief synopsis of the formalism in the next section while a more thorough and detailed development can be found in [26] and [27].

THE NEGF FORMALISM

Isolated system

An isolated device and its energy levels are described using a Hamiltonian H, a Hartree potential U and energy eigen-states of the electron, α.

$$(H + U)\psi_\alpha(\vec{r}) = \varepsilon_\alpha \psi_\alpha(\vec{r}). \qquad (1)$$

The potential U is obtained using Poisson's equation and accounts for the effect of any change in the density matrix on the channel capacitance. The channel capacitance consists of an electrostatic capacitance that depends on the dielectric constant ε_r and a quantum capacitance which depends on the density of eigen states in the channel [27]. The electron density matrix in real space is given by

$$\left[\rho(\vec{r}, \vec{r}')\right] = \int_{-\infty}^{+\infty} dE f(E - \mu)\delta([EI - H]). \qquad (2)$$

$\delta(EI\text{-}H)$ is the local density of states. Using the standard expansion for the delta function we get

$$\delta(EI - H) = \frac{i}{2\pi}\left(\left[\left(E + i0^+\right)I - H\right]^{-1} - \left[\left(E - i0^+\right)I - H\right]^{-1}\right). \qquad (3)$$

From the above equation, the delta function can also be written as

$$\delta(EI - H) = \frac{i}{2\pi}\left[G(E) - G^+(E)\right];$$

$$G(E) = \left[\left(E - i0^+\right)I - H\right]^{-1}. \qquad (4)$$

$G(E)$ is the retarded Green's function while $G^+(E)$, its conjugate complex transpose, is called the advanced Green's function. In the time domain, the Green's function can be interpreted as the impulse response of the Schrödinger equation that will give us the nth component of the wave function if the system is given an impulse excitation at the mth component. In the energy domain the Green's function gives the energy eigen-values for the eigen-states that are occupied in response to the applied impulse. The diagonal elements of the spectral function, which is the difference between the retarded and advanced Green's function, represent the occupied local electron density of states.

$$A(\vec{r}, \vec{r}', E) = 2\pi\delta(EI - H) = i\left[G(E) - G^+(E)\right]. \qquad (5)$$

Thus the electron density matrix for an isolated device can also be written in the form

$$[\rho] = \int_{-\infty}^{+\infty} \frac{dE}{2\pi} f(E - \mu)[A(E)]. \qquad (6)$$

Open system

Now consider the case of an open system consisting of a channel connected to source and drain contacts. Let μ_1 and μ_2 be the chemical potentials of the source and the drain. The distribution of electrons in the semi-infinite source and drain is said to follow the Fermi distribution. For a two dimensional film the Fermi function is given by considering the electrons to have periodic boundary in the infinite x and y directions and experience confinement along the z direction.

$$f_{2D} = N_0 \ln\left(1 + \exp\left(-E/k_B T\right)\right) \text{ where } N_0 = \frac{m_c k_B T}{2\pi\hbar^2}. \qquad (7)$$

The difference in the Fermi levels of the source and drain causes electrons to flow from the source to the drain through the channel. When no scattering is incorporated the channel can be considered to be ballistic in nature and is expected to have zero resistance to current flow. However, experimental measurements [28] have shown that the maximum measured conductance of a one-energy level channel approaches a limiting value $G_0 = 2q^2/\hbar = 51.6(K\Omega)^{-1}$. The reason for this limit to conductance arises from the fact that current in the contacts is carried by infinite transverse modes while the number of available modes in the channel is limited. This means that the density of states in the contacts is spread over a large energy range while the channel density of states lies specifically between μ_1 and μ_2. Upon coupling the contact and the channel, some of the density of states from the contact spread into the channel while the channel loses some of its density of states to the contact. As a result, the coupling causes the density of states in the channel to spread out over a wider range of energy levels resulting in a reduction in the number of states lying between μ_1 and μ_2. Consequently, the overall effect of the coupling is to broaden the range of energy levels of the channel leading to a reduction in the number of states in the range μ_1 to μ_2 that are available for electron flow through the channel. In the NEGF formalism the coupling of the device to the source and drain contacts is described using self-energy matrices Σ_1 and Σ_2. The self-energy term can be viewed as a modification to the Hamiltonian to incorporate the boundary conditions. Accordingly, equation 1 and 4 can be rewritten as

$$\left(H + U + \Sigma_1 + \Sigma_2\right)\psi_\alpha(\vec{r}) = \varepsilon_\alpha \psi_\alpha(\vec{r}) \qquad (8)$$

$$G(E) = \left[\left(E - i0^+\right)I - H - \Sigma_1 - \Sigma_2\right]^{-1}. \qquad (9)$$

The self-energy term originates from the solution of the contact Hamiltonian. In this semi-infinite system, which is connected to the channel, there will be an incident wave from the channel as well as a reflected wave from the contact. The wave function at the interface is matched to conserve energy giving the boundary condition

$$\Sigma_i = -t\exp(ika) \qquad (10)$$

where t is a result of the discretization and is given by

$$t = \frac{-\hbar^2}{2m^*a^2}. \qquad (11)$$

The broadening of the energy levels introduced by connecting the device to the source and drain contacts is incorporated through the Gamma functions Γ_1 and Γ_2 given by

$$\Gamma_1 = i(\Sigma_1 - \Sigma_1^+) \qquad \Gamma_2 = i(\Sigma_2 - \Sigma_2^+) \qquad (12)$$

The electron density for the open system is given by

$$[\rho] = \int_{-\infty}^{+\infty} \left(\frac{dE}{2\pi}\right)[G^n(E)]. \qquad (13)$$

$G^n(E)$ represents the electron density per unit energy and is given by

$$G^n = G\Sigma^{in}G^+ \quad \text{where} \quad [\Sigma^{in}] = [\Gamma_1]f_1 + [\Gamma_2]f_2. \qquad (14)$$

Electron-phonon coupling

An electron in a device can interact with its surroundings elastically or inelastically depending on the nature of surroundings. Elastic interactions occur when the surroundings are rigid leading to energy and momentum conservation. Such interactions are coherent in nature. Inelastic interactions occur when energy is dissipated through the emission or absorption of phonons, photons, etc. Such types of interactions are known as incoherent or phase-breaking processes. Inelastic scattering is in general difficult to model exactly. In this paper we treat the phase-breaking scattering to be nearly elastic, i.e. $E \approx E + \hbar\omega \approx E - \hbar\omega$. The effect of scattering is incorporated into the coherent model discussed previously by treating it as another contact where electrons enter and leave the contact leading to no net current at that contact [26]. However, because the scattering terminal does not have a defined Fermi level, the scattering terms Σ_s and Σ_s^{in} have to be determined through other means. As such

$$\Sigma_s^{in}(\vec{r},\vec{r}';E) = D_o G^n(\vec{r},\vec{r}';E) \qquad (15)$$

$$\Gamma_s(E) = D_o A(E), \text{ and } \Sigma_s(E) = D_o G(E). \qquad (16)$$

D_o is defined as the phonon correlation function and is calculated using the phonon deformation potential and the phonon wave vector β.

$$D_o(\vec{r},\vec{r}',\hbar\omega) = \sum_\beta \delta\left(E - \hbar\omega(\vec{\beta})\right)U_\beta(\vec{r})U_\beta^*(\vec{r}') \qquad (17)$$

$$U_\beta(\vec{r}) = U_\beta \exp(i\vec{\beta}.\vec{r}) \text{ where } U_\beta = D_{ADP}\beta\sqrt{\frac{2\hbar}{\rho\omega\Omega}} \qquad (18)$$

U_β is the interaction potential while D_{ADP} is the acoustic deformation potential. ρ is the mass density and Ω is the normalization volume. Depending on the system temperature there are a wide range of phonons with which electrons scatter. However in our model we use a simplified case of the electrons interacting with phonons of a single frequency in an attempt to illustrate the effect of scattering on electron transport in devices. For example $Do = 0.1eV^2$ corresponds to a phonon energy of 20meV [27]. This phonon energy is not related to the temperature of the device. In fact, the NEGF model does not include temperature within the system as temperature can be expressed only for a system that is in equilibrium. The only place where temperature is included in the model is in the source and drain Fermi functions. Instead, the phonon energy represents the dominant phonon frequency available for scattering [13]. In the present model we assume D_{ADP} is independent of the electron energy in the channel and corresponds to optical phonon scattering only, which is expected to be the dominant electron scatterer [27].

The source, drain and scattering self-energy terms are used to obtain the final Green's function from which the net current at each contact is calculated as a difference in the inflow and outflow currents using equation 19. The entire calculation is carried out self-consistently with Poisson's equation to account for the change in channel potential with the change in electron density.

$$I_i = \frac{-q}{\hbar}\int_{-\infty}^{+\infty} Trace[\Gamma_i A]f_i - Trace[\Gamma_i G^n] \qquad (19)$$

RESULTS

**Thermoelectric effects in Si/Ge/Si quantum well structure**

The device under study consists of a single quantum well formed by alternating layers of silicon, germanium and silicon thin films as shown in Figure 1. The thickness of each film is 20Å. Electron confinement in the device occurs due to two reasons. 1) The very small thickness of the films gives rise to discretely spaced energy subbands in the cross-plane direction. 2) For constant doping levels in all three layers, the larger bandgap of the silicon layers on either side of the germanium layer sets up a potential barrier for the electrons in germanium thus causing additional confinement of the electrons in germanium leading to a 1D potential well. Electron transport in the device under an applied bias is modeled along the confined z direction. The Seebeck coefficient for the well was studied for various temperature ranges of the source and drain contacts while varying the doping in the Si/Ge/Si well. The source temperature was maintained constant at 300K while the drain contact was maintained a higher temperature relative to the source. The applied bias ranged from 0 to 0.1V.
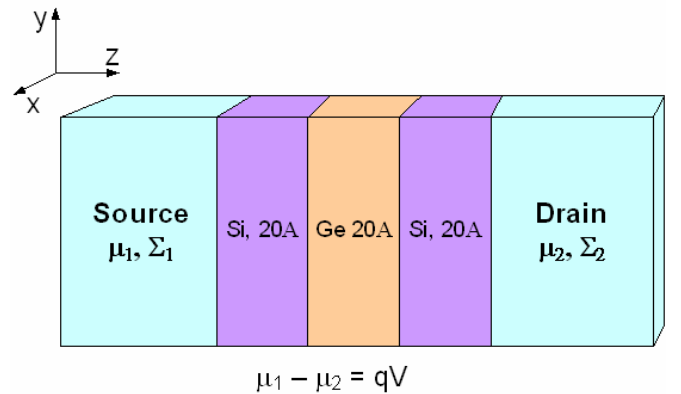
Figure 1. Schematic representation of the nanodevice modeled in the simulation. E is the electron energy in the device while Σ_s is the scattering self energy.

Figure 2 shows the current-voltage characteristics for a ballistic quantum well doped to a concentration of $5\times10^{18}cm^{-3}$. The

source-drain temperature difference ranges from 0K to a maximum of 30K. The temperature gradient results in a diffusion of electrons towards the source, opposing the direction of the bias leading to negative current values. As bias is increased, electrons from the source are drawn towards the drain and, at the Seebeck voltage, balance the flow of electrons due to the temperature gradient leading to zero current values. The electrical conductivity for the films is calculated using the gradient of the linear portion of the current density-voltage curve (seen in Figure 2).
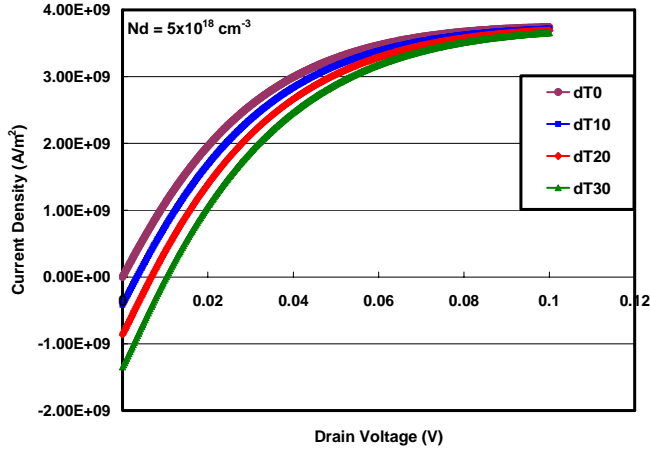
Figure 2. Current density - voltage characteristics of a ballistic Si(20Å)/Ge(20Å)/ Si(20Å) quantum well structure. Channel temperature difference ranges from 0K to 30K.

Figure 3 shows the predicted and measured Seebeck coefficient values found in the literature as a function of doping levels for Si/Ge/Si quantum well superlattices. The agreement between the calculated results and experiments is remarkable considering the limitations of the model and uncertainty of several experimental parameters that will be discussed shortly.

Figure 4 shows the current-voltage characteristics of the superlattice with scattering. While the presence of dopant atoms can lead to impurity scattering, as mentioned in the introduction, we have considered electron energy-independent near-elastic phonon scattering for this study. In the scattering model considered the free parameter Do was varied from very low phonon energy of 2meV to 60meV, which is the optical phonon energy limit in the case of silicon, and the I-V characteristics were collected. Inclusion of electron-phonon scattering caused a significant drop in the current conducted through the channel indicating increased resistance to current flow with scattering as seen from Figure 4. While the electrons do not lose any energy to the lattice, they experience a momentum redistribution which in turn increases the resistance to current flow. Under such circumstances the Seebeck coefficient does not change as electrons do not undergo any energy change. Our current research efforts are focused towards a full inelastic scattering model and the results will be published as soon as they become available.

Figure 5 shows the electrical conductivity σ values for incoherent near-elastic scattering for doping levels of $5 \times 10^{18} cm^{-3}$ and $5 \times 10^{19} cm^{-3}$. For a Do value of 0.3 eV^2,

corresponding to phonon energy of 60meV (optical phonon energy range) the value of σ dropped by 77% of the ballistic value demonstrating the significance of electron-phonon scattering on the electrical conductivity.
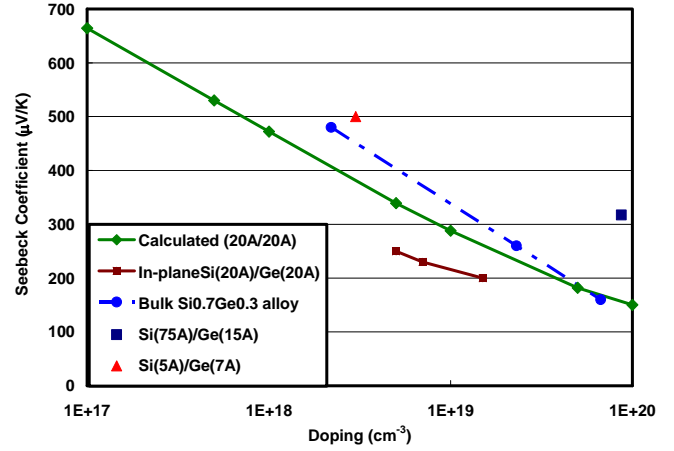

Figure 3. Seebeck coefficient vs. doping for Si/Ge/Si superlattices. Experimental data taken from [11, 29, 30, 31].

A number of factors need to be considered while comparing the experimental data to the results calculated by the NEGF model. 1) The superlattices used in the experiments consist of 300 to 1200 alternating layers of silicon and germanium films having thicknesses of the order of a few angstroms while our calculations using the NEGF model was done on a single quantum well with film thickness of 20Å each. While there is a paucity of experimental data for single layered Si/Ge/Si films in the cross-plane direction, there is a broad variation in the reported Seebeck coefficient and electrical conductivity for multi-layered Si/Ge/Si superlattices with thickness and doping levels. 2) The experimental data for the Seebeck coefficient and electrical conductivity report a spread in the actual doping values used in the thin films. The effect of this spread on the Seebeck coefficient is evident in Figure 3 from the plot for the calculated Seebeck coefficient vs. doping. It can be seen that a small change in doping level leads to a significant change in the S values demonstrating the uncertainty of the reported data. 3) The calculated σ values for the ballistic as well as scattering cases are in general lower than the experimentally reported values [31, 32]. It must be noted that the electrical conductivity values used in [31] are an ad-hoc estimate from the in-plane electrical conductivity values. One practice to calculate the cross-plane electrical conductivity is to divide the measured in-plane electrical conductivity by the ratio of the in-plane/cross-plane thermal conductivity [32]. Some experiments also report data measured at high temperatures [32] to overcome the effect of the large contact resistance prevalent in nanoscale devices. While such data is more representative of the material properties of the superlattice, it is important to include the effect of the contacts to better understand the performance of superlattices as thermoelectric devices. In the NEGF model, the effect of the contacts is included through the broadening terms Γ_1 and Γ_2.

5
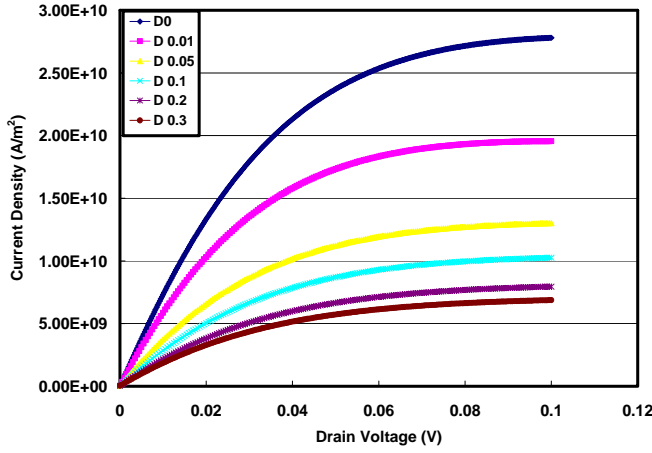
Figure 4. Current density vs. voltage characteristics for incoherent near-elastic scattering for Si/Ge/Si superlattice for Nd = 5x10^19 cm^-3.

4) It is seen from our simulations that the values used for the effective mass for silicon and germanium were found to have a significant effect on the predicted electrical conductivity values. For our calculations we used the effective mass corresponding to bulk conductivity values while the various experiments were performed on single crystalline epitaxial layers deposited on a graded Si_xGe_{1-x} substrate. For film thicknesses of the order of a few nanometers as used in our calculations, both silicon and germanium can be considered to be single crystals allowing us to use the effective mass for that particular orientation. In addition, the graded substrate used in the experiments introduces lateral strains in the silicon and germanium films changing the lattice constant and the effective mass. There is however very limited data available on the change in effective mass with these strained and unstrained substrates.
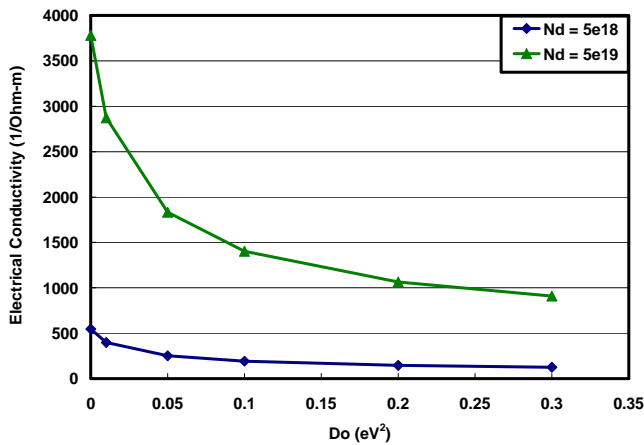
Figure 5. Electrical conductivity (sigma) values for incoherent near-elastic scattering for doping levels of 5x10^18 cm^-3 and 5x10^19 cm^-3.

The power factor $S^2\sigma$ was calculated using the conductance values for each level of scattering along with the Seebeck coefficient obtained for each doping level considered. While the electrical conductivity increases with doping in general it

can be seen that the increase in electrical conductivity with doping is more than compensated by the decrease in electrical conductivity due to electron-phonon scattering. As a result, the overall power factor value dropped to 23% of the ballistic value for the Si(20Å)/Ge(20Å)/Si(20Å) quantum well superlattice.
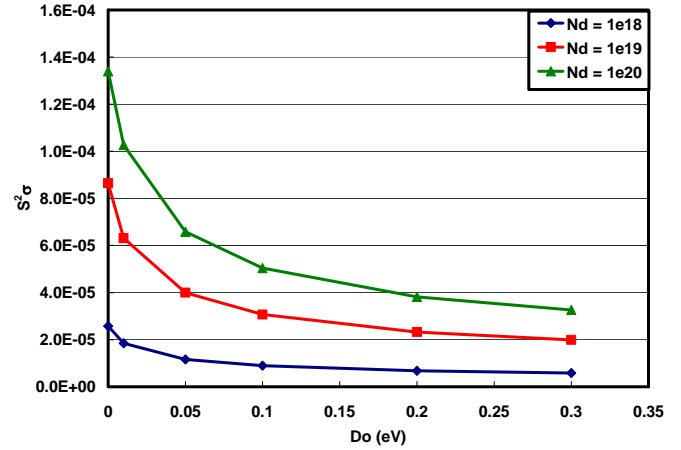
Figure 5. Change in the power factor $S^2\sigma$ with incoherent near-elastic scattering for Si/Ge/Si superlattice for three different doping levels.

CONCLUSIONS

The non-equilibrium Green's function formalism was used to study the coupled effects of quantum confinement and scattering on the thermoelectric behavior of a single Si(20Å)/Ge(20Å)/Si(20Å) quantum well superlattice. While increased confinement is believed to decrease the thermal conductivity due to phonon confinement and interface scattering, the perceived gains due to decreased thermal conductivity do not translate into a corresponding improvement in the figure of merit ZT. While electron confinement is believed to play an important role in decreasing the electrical conductivity electron-phonon scattering is also believed to contribute significantly to this decrease despite the near ballistic nature of electron transport. Using the nonequilibrium Green's function to successfully couple quantum and scattering effects it was seen that for phonon energies in the optical range increased resistance due to scattering decreased the overall power factor by 77%.

ACKNOWLEDGMENTS

REFERENCES

[1] Tritt, T. M., Mahan, G., Kanatzidis, M. G., Nolas, G. S. and Mandrus, D., 2001, "Thermoelectric Materials 2000. The Next Generation Materials for Small-Scale Refrigeration and Power Generation," *Material Research Society*, **626**.

[2] Hicks, L.D. and Dresselhaus, M. S., 1993, "Effect of Quantum Well Structures on the Thermoelectric Figure of Merit," *Physical Review B*, **47**, **12**, pp. 727-731.

[3] Whitlow, L. W. and Hirano, T., 1995, "Superlattice Applications to Thermoelectricity," *Journal of Applied Physics*, **78**, **9**, pp.5460-5466.

[4] Hicks, L. D., Harman, T. C. and Dresselhaus, M. S., 1993, "Use of Quantum-well Superlattices to Obtain a High Figure of Merit from Non-conventional Thermoelectric Materials," *Applied Physics Letters*, **63**, **23**, pp.3230-3232.

[5] Tritt, T. M., 2001, "Recent Trends in Thermoelectric Materials Research III," *Semiconductors and Semimetals*, **71**, Academic Press, London.

[6] Balandin, A and Wang, K. L., 1998, "Significant decrease of the lattice thermal conductivity due to phonon confinement in a free-standing semiconductor quantum well," *Physical Review B*, **58**, **3**, pp. 1544-1549.

[7] Balandin, A and Wang, K. L., 1998, "Effect of phonon confinement on the thermoelectric figure of merit of quantum wells," *Journal of Applied Physics*, **84**, **11**, pp. 6149-6153.

[8] Simkin, M. V, and Mahan, G. D., 2000, "Minimum Thermal Conductivity of Superlattices," *Physical Review Letters*, **84**, **5**, pp. 927- 930.

[9] Chen, G., 1998, "Thermal Conductivity and Ballistic-Phonon Transport in the Cross-Plane Direction of Superlattice," *Physical Review B*, **57**, **23**, pp. 14958-14973.

[10] Chen, G., 1999, "Phonon Wave Heat Conduction in Thin Films and Superlattices," *Journal of Heat Transfer*, **121**, pp. 945-953.

[11] Koga, T., Cronin, S. B., Dresselhaus, M. S., Liu, J. L. and Wang, K. L., 2000, "Experimental proof-of-principle Investigation of enhanced $Z_{3D}T$ in 001 oriented Si/Ge superlattices," *Applied Physics Letters*, **77**, **10**, pp. 1-3.

[12] Dresselhaus, M. S., 2003, "Nanostructures and energy conversion," *Proceedings of 2003 Rohsenhow Symposium on Future Trends of Heat Transfer*.

[13] Lundstrom, M. S., 2000 "*Fundamentals of Carrier Transport*," Cambridge University Press, New York.

[14] Packan, P. A., 1999, "Pushing the Limits," *Science*, **285**, pp. 2079–2080.

[15] Rahman, A., Ghosh, A and Lundstrom, M., 2003, "Assessment of Ge n-MOSFETs by Quantum Simulation," *Technical Digest of International Electronic Devices Meeting*, pp. 471-473.

[16] Mazumder, P., Kulkarni, S., Bhattacharya, M., Sun, J. P. and Haddad, G.I., 1998, "Digital Circuit Applications of Resonant Tunneling Devices," *Proceedings of the IEEE*, **86**, **4**, pp. 664-686.

[17] Lugli, P. 1990, "The Monte Carlo Method for Semiconductor Device and Process Modeling." *IEEE transactions on computer-aided design of integrated circuits and systems*, **9**, **11**, pp.1164–1176.

[18] Mazumder, S and Majumdar, A., 2001, "Monte Carlo Study of Phonon Transport in Solid Thin Films including Dispersion and Polarization," *Journal of Heat Transfer*, **123**, pp.749–759.

[19] Lai, J and Majumdar, A., 1996, "Concurrent Thermal and Electrical Modeling of Sub-micrometer Silicon Devices," *Journal of Applied Physics*, **79**, **9**, pp.7353–7361.

[20] Raman, A., Walker, D. G. and Fisher, T. S., 2003, "Simulation of Nonequilibrium Thermal Effects in Power LDMOS Transistors," *Solid-State Electronics*, **47**, **8**, pp.1265–1273.

[21] Murthy, J. Y. and Mathur, S. R., 2002, "Computation of Sub-micron Thermal Transport Using an Unstructured Finite Volume Method," *Journal of Heat Transfer*, **124**, **6**, pp.1176–1181.

[22] Asenov, A., Watling, J. R., Brown, A. R. and Ferry, D. K., 2002, "The Use of Quantum Potentials for Confinement and Tunneling in Semiconductor Devices," *Journal of Computational Electronics*, **1**, pp.503–513.

[23] Tang, T. W. and Wu, B., 2004, "Quantum Correction for the Monte Carlo Simulation via the Effective Conduction-band Edge Equation," *Semiconductor Science and Technology*, **19**, pp. 54-60.

[24] Lent, C., S. and Kirkner, D., J., 1990, "The Quantum Transmitting Boundary Method," *Journal of Applied Physics*, **67**, **10**, pp. 6353-6359.

[25] Laux, S., E., Kumar, A. and Fischetti, M., V., 2002, "Ballistic FET Modeling Using QDAME: Quantum Device Analysis by Modal Evaluation," *IEEE Transactions on Nanotechnology*, **1**, **4**, pp. 255-259.

[26] Datta, S., 2000, "Nanoscale Device Simulation: The Green's Function Formalism," *Superlattices and Microstructures*, **28**, pp. 253-278.

[27] Datta, S., 2005, "*Quantum Transport: Atom to Transistor*," Cambridge University Press, New York.

[28] Szafer, A. and Stone, A. D., 1989, "Theory of Quantum Conduction through a Constriction," *Physical Review Letters*, **62**, pp. 300-303.

[29] Dismukes, J. P., Ekstrom, L., Steigmeier, E. F., Kudman, I. and beers, D. S., 1964, "Thermal and Electrical Properties of Highly Doped Ge-Si Alloys upto 1300^0K", *Journal of Applied Physics*, **10**, **35**, pp. 2899-2907.

[30] Yang, B., Liu, J. L., Wang, K. L. and Chen, G., 2002, "Simultaneous measurements of Seebeck coefficient and thermal conductivity across superlattice," *Applied Physics Letters*, **80**, **10**, pp. 1758-1760.

[31] Yang, B., Liu, J., Wang, K. and Chen, G., 2001, "Characterization of Cross-Plane Thermoelectric Properties of Si/Ge Superlattices", *Proceedings of 20th International Conference on Thermoelectrics*.

[32] Yang, B., Liu, W. L., Liu, J. L., Wang, K. L. and Chen, G., 2002, "Measurements of Anisotropic Thermoelectric Properties in Superlattices," *Applied Physics Letters*, **81**, **19**, pp. 3588-3590.